# Gas hydrate growth and dissociation in narrow pore networks: capillary inhibition and hysteresis phenomena

R. ANDERSON*, B. TOHIDI & J. B. W. WEBBER

*Centre for Gas Hydrate Research, Institute of Petroleum Engineering, Heriot–Watt University, Edinburgh, EH14 4AS, UK*

**Corresponding author (e-mail: ross.anderson@pet.hw.ac.uk)*

**Abstract:** Marine sediments hosting gas hydrates are commonly fine-grained (silts, muds, clays) with very narrow mean pore diameters (~0.1 μm). This has led to speculation that capillary phenomena could play an important role in controlling hydrate distribution in the seafloor, and may be in part responsible for discrepancies between observed and predicted (from bulk phase equilibria) hydrate stability zone (HSZ) thicknesses. Numerous recent laboratory studies have confirmed a close relationship between hydrate inhibition and pore size, stability being reduced in narrow pores; however, to date the focus has been hydrate *dissociation* conditions in porous media, with capillary controls on the equally important process of hydrate *growth* being largely neglected. Here, we present experimental methane hydrate growth and dissociation conditions for synthetic mesoporous silicas over a range of pressure–temperature (*PT*) conditions (273–293 K, to 20 MPa) and pore size distributions. Results demonstrate that hydrate formation and decomposition in narrow pore networks is characterized by a distinct hysteresis: solid growth occurs at significantly lower temperatures (or higher pressures) than dissociation. Hysteresis takes the form of repeatable, irreversible closed primary growth and dissociation *PT* loops, within which various characteristic secondary 'scanning' curve pathways may be followed. Similar behaviour has recently been observed for ice–water systems in porous media, and is characteristic of liquid–vapour transitions in mesoporous materials. The causes of such hysteresis are still not fully understood; our results suggest pore blocking during hydrate growth as a primary cause.

Naturally occurring gas hydrates (or clathrate hydrates) in sediments may pose a hazard to deepwater drilling and production operations (Kvenvolden 1999; Milkov *et al.* 2000), have potential as a strategic low-carbon energy reserve (Kvenvolden 1999; Lee & Holder 2001), could provide a means for deep ocean $CO_2$ disposal through sequestration/storage (Hunter 1999; Brewer *et al.* 1999), and have long-term significance with respect to ocean margin stability, methane release to the atmosphere and global climate changes (Kvenvolden, 1999; Dickens, 2003).

Although our understanding of sediment-hosted gas hydrates has grown considerably in recent years, we still lack fundamental knowledge concerning the mechanisms of hydrate growth, accumulation and distribution within the subsurface. Clathrates have been recovered in shallow ocean floor sediment cores from numerous sites around the world (e.g. Ocean Drilling Program (ODP) Leg 164, Blake Ridge, offshore South Carolina (Paull *et al.* 2000), and Leg 204, Cascadia Margin, offshore Oregon (Tréhu & Shipboard Scientific Party 2003)). Sediments hosting gas hydrates are generally characterized by organic matter-rich fine-grained silts, muds and clays, with lesser coarser sandy layers present at some sites. Hydrates commonly display a wide range of growth habits, and are often patchily distributed within the host sediment according to texture (Booth *et al.* 1996). In fine-grained strata, hydrates are generally found in the form of segregated nodules, lenses, pellets or sheets. In contrast, where coarser layers are present, clathrates often form an interstitial pore fill between sediment grains. This variation in growth patterns according to sediment type suggests that host sediment properties may play an important role in controlling hydrate morphology and distribution within the subsurface (Clennell *et al.* 1999; Henry *et al.* 1999).

Further evidence for potential host sediment controls on hydrate equilibria comes from the predicted depth of the Base of the Hydrate Stability Zone (BHSZ) in seafloor sediments. While ODP coring has confirmed that the BHSZ commonly lies close to pressure and temperature conditions calculated from bulk (unconfined) phase equilibria, there are a number of sites where the thickness is notably less than predicted (e.g. Blake Ridge (Paull *et al.* 2000), and Cascadia Margin (Tréhu & Shipboard Scientific Party 2003)). The depth of the BHSZ is dependent on various factors, including

*From*: Long, D., Lovell, M. A., Rees, J. G. & Rochelle, C. A. (eds) *Sediment-Hosted Gas Hydrates: New Insights on Natural and Synthetic Systems*. The Geological Society, London, Special Publications, **319**, 145–159.
DOI: 10.1144/SP319.12 0305-8719/09/$15.00 

gas concentration (gas concentration must exceed aqueous equilibrium solubility in the presence of hydrate), composition (the addition of $CO_2$, $H_2S$ and higher thermogenic hydrocarbons such as ethane/propane increases hydrate stability), pore water salinity (dissolved salt reduces stability) and the local geothermal gradient. However, where these are relatively well established from drilling/coring (such as at the Blake Ridge and Cascadia Margin), additional factors must be sought to explain predicted/actual BHSZ discrepancies. One potential influence may be the host sediments themselves. The mechanisms by which sediment properties could alter hydrate stability and/or influence distribution are still relatively poorly understood (Max 2000); however, one potentially important factor which has received considerable attention in recent years is capillary inhibition (Clennell *et al.* 1999; Henry *et al.* 1999).

## Phase behaviour in confined geometries

It is well established that the pressure–temperature (*PT*) conditions of first-order phase transitions (e.g. solid–liquid, liquid–vapour) may be significantly altered in confined geometries. In narrow pores, high-curvature phase interfaces can induce strong differential capillary pressures, altering the chemical potential of components relative to bulk (unconfined) conditions. For solid–liquid transitions, where pore sizes are sufficient for phases to retain the structural and physical properties of the bulk phase, solid melting temperatures are generally depressed as a function of pore radius in accordance with the Gibbs–Thomson equation (the constant pressure analogue of the constant temperature Kelvin equation for vapour pressure in mesoporous media; (Enüstün *et al.* 1978; Christensen 2001). For simple, single-component systems (e.g. ice–water), the common form of the equation relates the pore solid melting point depression, $\Delta T_p$, from the bulk (unconfined) melting temperature, $T_b$, to the pore radius, $r$, through:

$$\Delta T_p = T_b \cdot \frac{F\gamma_{sl} \cos\theta}{r\rho_l \Delta H_{sl}} \quad (1)$$

where $\gamma_{sl}$ is the solid–liquid interfacial free energy (often referred to as the surface or interfacial tension), $F$ the shape factor of the interface (dependent on interface curvature), $\rho_l$ the density of the liquid phase, $\Delta H_{sl}$ the latent heat (enthalpy) of fusion, and $\theta$ the contact angle between the solid phase and the pore wall (180° measured inside the solid phase if an unfrozen liquid layer is assumed, thus $\cos\theta = -1$). Where $\gamma_{sl}$ and $\Delta H_{sl}$ are relatively constant over the *PT* conditions of interest, equation (1) dictates a linear relationship between $\Delta T_p/T_b$ and reciprocal pore radius, as confirmed experimentally for many organic and inorganic liquids (Rennie & Clifford 1977; Jackson & McKenna 1990, 1996; Christensen 2001). It should be noted that equation (1) assumes that the solid phase pressure ($P_s$) is equal to the bulk pressure ($P_b$), that is, $P_l < P_s = P_b$. Where the liquid phase ($P_l$) is at bulk pressure ($P_s > P_l = P_b$), the value $\rho_l$ should be replaced by $\rho_s$, the density of the solid phase (Enüstün *et al.* 1978).

Although the thermodynamics of solid–liquid equilibria in small pores (particularly ice–water equilibria) has been the subject of investigation for over 100 years (Christensen 2001), only relatively recently did Handa & Stupin (1992) demonstrate that methane hydrate dissociation temperatures are depressed in narrow pores. Seafloor sediments hosting gas hydrates are commonly fine-grained (silts, muds, clays), with narrow mean pore diameters (~0.1 μm; Griffiths & Joshi 1989; Clennell *et al.* 1999). In light of this, it has previously been speculated that capillary phenomena could play an important role in controlling hydrate stability and distribution within sediments, and may be partly responsible for observed discrepancies between predicted and actual BHSZs (Ruppel 1997; Clennell *et al.* 1999; Henry *et al.* 1999).

In the most extensive theoretical analyses to date, Clennell *et al.* (1999) & Henry *et al.* (1999) (companion papers) developed a capillary-thermodynamic model for hydrate formation in the seafloor which attempted to account for the effect of pore size on equilibrium conditions. From model predictions, the authors could not confirm that capillary inhibition alone was responsible for observed discrepancies between predicted and actual BHSZs, although it was concluded that capillary phenomena did most likely play an important role in controlling hydrate phase behaviour and distribution, particularly in segregation and lens/nodule/layer formation. A lack of firm conclusions concerning the extent to which pore size affects the HSZ could in part be attributable to a lack of available values for hydrate–liquid (water) interfacial free energy (the authors used a value for ice–water interfacial free energy), and, significantly, an absence of reliable data relating pore size/geometry to hydrate growth/dissociation conditions with which to validate model predictions.

The potential role capillary effects may have in controlling hydrate growth and accumulation within sediments has led to considerable experimental and theoretical research into the phenomenon over the past 8 years. Work has focused primarily on (relatively) well characterized porous silicas (Uchida *et al.* 1999, 2002; Seshadri *et al.* 2001; Wilder *et al.* 2001*a*, *b*; Seo *et al.* 2002; Smith

*et al.* 2002*a*, *b*, 2004; Wilder & Smith 2002; Zhang *et al.* 2002, 2003; Seo & Lee, 2003; Aladko *et al.* 2004; Dicharry *et al.* 2005), and more recently on natural sands and clays (Uchida *et al.* 2004). Although there are a number of discrepancies between studies, particularly regarding experimental data interpretation (as discussed by Anderson *et al.* 2003*a*), the overall conclusion is that narrow pores have a significant and consistent inhibiting effect on hydrate stability. However, phase behaviour in porous media is highly complex, and there are many potentially important factors that have not yet been addressed. One significant, and particularly relevant, issue is that the focus to date has been the measurement and prediction of hydrate *dissociation* conditions in porous media, with the equally, if not more important process of hydrate *growth* being largely overlooked.

As suggested by Clennell *et al.* (1999), capillary theory predicts a considerable hysteresis may exist between solid growth and melting conditions in narrow pores. The hysteresis loops commonly associated with gas (e.g. nitrogen) adsorption/desorption in mesoporous materials and hydrocarbon reservoir rock drainage/imbibition curves are testament to the fact that such behaviour is a common characteristic of capillary pressure controlled phase transitions and fluid flow within porous media.

In Anderson *et al.* (2003*b*), we reported experimental $CH_4$, $CO_2$ and $CH_4$–$CO_2$ clathrate hydrate dissociation and ice melting data for mesoporous silica glasses. This data was used to estimate values for ice–water and hydrate–liquid (water) interfacial free energies through a modified version of equation (1), and subsequently employed to validate a capillary corrective function for hydrate thermodynamic models which allows the prediction of hydrate dissociation conditions for narrow cylindrical- or spherical-like pores (Llamedo *et al.* 2004). The added effect of pore water salinity was also investigated (Østergaard *et al.* 2002). Here, we report the results of a detailed experimental investigation of methane hydrate *growth and dissociation* conditions in synthetic mesoporous silica glasses. Data reveal an equilibrium hysteretic hydrate formation/decomposition behaviour not previously observed for clathrates in porous media. Through an analysis of experimental data, we will assess potential origins of the observed hysteresis phenomena, and then comment briefly on potential implications for seafloor hydrate systems.

## Experimental equipment and methods

A specifically designed high-pressure (max. 41 MPa) set-up was used in experiments. The set-up, shown in Figure 1, consists of an equilibrium cell (75 $cm^3$ volume) with removable sample cup, central PRT (platinum resistance thermometer), inlet/outlet valve, Quartzdyne pressure transducer and insulated coolant jacket.

The PRT was calibrated with a Prima 3040 precision thermometer, and measures cell temperature to $\pm 0.01$ K with an estimated accuracy of $\pm 0.1$ K. The transducer, via a computer interface, can measure system pressure to within $\pm 6.9 \times 10^{-6}$ MPa, and has a quoted accuracy of $\pm 0.008$ MPa for the complete operating range of 0–138 MPa. System temperature was controlled by circulating fluid from a programmable cryostat (253–373 K) through the cell jacket, and could be kept stable to within $\pm 0.02$ K. Cell temperature and pressure were continuously monitored and recorded using a computer.

Double-distilled water was used in all experiments. High-purity methane (99.995 mol%) was

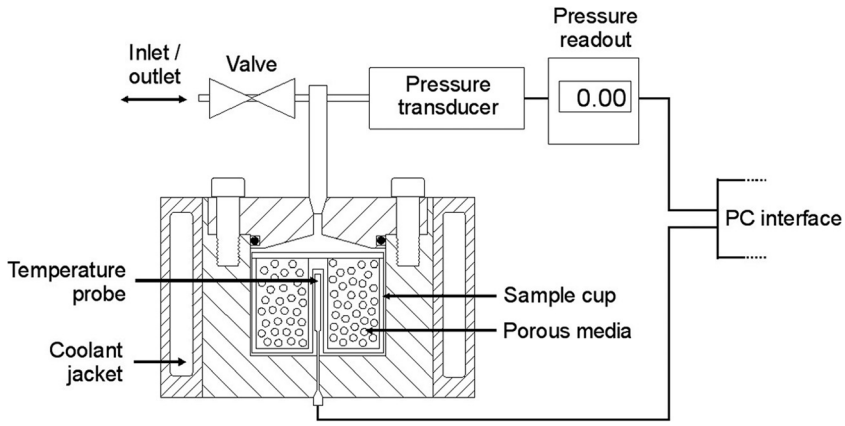


**Fig. 1.** Schematic illustration of the high-pressure set-up used in experiments.

supplied by Air Products. Porous silica samples, known as Controlled Pore Glass (CPG), were purchased from CPG Inc., USA (now Millipore, USA), and consist of 37–74 μm porous silica shards. Three samples, of 30.6, 15.8 and 9.2 nm nominal pore diameters, were used for experiments. Sample pore size distributions were previously characterized independently by NMR (nuclear magnetic resonance) cryoporometry (Anderson *et al.* 2003*b*; Dore *et al.* 2004).

Test procedures were as follows. CPG silicas were dried overnight in an oven, then saturated (water volume, $V_w >$ pore volume, $V_p$) with a measured volume of distilled water. Prepared samples were placed in the cell, the cell cooled and water frozen (to minimize evaporation), then air evacuated. Temperature was subsequently raised again to the desired starting temperature (generally outside the bulk hydrate stability zone) before methane was injected to the initial starting pressure. To form hydrates in the first instance, the cell was cooled rapidly until growth commenced, as indicated by pressure–temperature relations. Subsequent to this, hydrate growth and dissociation *PT* pathways for sample hysteresis regions were determined by a stepped temperature cycling method based on the approach of Tohidi *et al.* (2000) & Anderson *et al.* (2003*b*). The method involves heating/cooling of the cell in steps (generally 0.2–0.5 K), with sufficient time being given (in this case 8–24 h) for the system to reach equilibrium (as indicated by stable pressure) following each step, which results in very reliable and highly repeatable (to within ±0.1 K) measurements.

## Results and discussion

Equilibrium methane hydrate growth and dissociation conditions were determined at various pressures for the three different CPG silica samples (30.6, 15.8 and 9.2 mean pore diameters). Figure 2 shows an example of typically observed clathrate growth and dissociation pressure–temperature pathways, in this case for the 30.6 nm sample. As system water volume exceeds CPG pore volume, gas hydrates form both within and outside the pore network; hydrates outwith the pores dissociate at the bulk (unconfined) methane hydrate + liquid + gas (H + L + G) phase boundary, with both pore

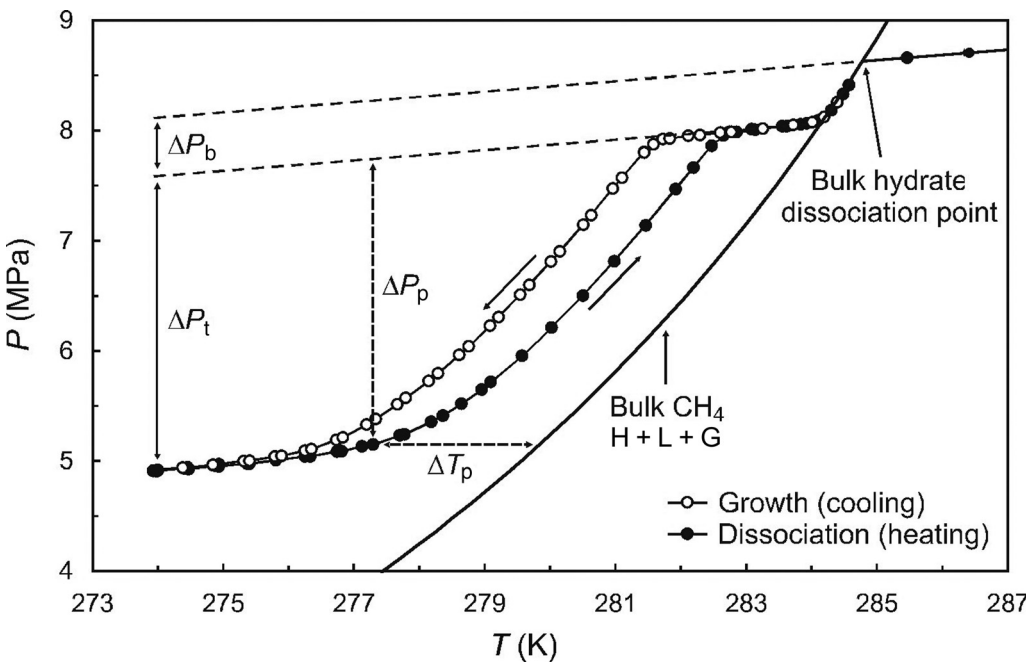


**Fig. 2.** Plot of primary growth and dissociation *PT* data for the 30.6 nm mean pore diameter CPG silica saturated with water. $\Delta P_t$ and $\Delta P_b$ are the total change in pressure associated with hydrate formation in the pores and the bulk respectively. $\Delta T_p$ and $\Delta P_p$ are the temperature depression of pore hydrate/growth dissociation conditions (from the bulk methane H + L + G phase boundary) and change in pressure associated with pore hydrate formation at any given recorded equilibrium *PT* condition on the heating/cooling curves respectively. Bulk $CH_4$ data: polynomial fit to Deaton & Frost (1946), McLeod & Campbell (1961).

hydrate growth and dissociation conditions being depressed to significantly lower temperatures. The hysteresis between pore clathrate growth and dissociation conditions is distinct – hydrate formation occurs at temperatures significantly lower than decomposition, with irreversible (unidirectional) *PT* pathways forming a complete closed hysteresis loop. To our knowledge, this clear, repeatable (in the same closed system over 6 months), equilibrium *PT* hysteresis between growth and dissociation has not previously been reported for clathrate hydrates in porous media. Similar (although not so consistently repeatable) equilibrium hysteretic behaviour has been described for ice–water transitions in hardened cement pastes (Schulson *et al.* 2000; Swainson & Schulson 2001), however it is generally not reported in most literature studies of solid–liquid transitions in mesoporous materials.

In contrast to the repeatable, equilibrium hysteresis observed here, significant differences between measured freezing and melting temperatures due to stochastic heterogeneous nucleation phenomena have been reported for fluids confined to porous materials (Faivre *et al.* 1999; Morishige & Kawano 1999). In this case, hysteresis can be attributed to kinetic issues arising as a result of the supercooling generally required to initiate solid nucleation in the absence of a pre-existing crystalline phase. Here, we have eliminated the need for nucleation by ensuring clathrate is present in the bulk (outside the pores) when cooling to initiate pore hydrate growth. Theoretically, this means only progressive solid growth front propagation into media on cooling is required.

### *Characteristics of hysteresis loops*

From Figures 2 and 3, we see that primary pore hydrate dissociation and growth patterns are characterized by a sigmoidal (with respect to linear liquid + gas only *PT* relationships) curves indicative of formation/decomposition across a Gaussian-like distribution of pores typical of Controlled Pore Glasses (Anderson *et al.* 2003*a*, *b*; Østergaard *et al.* 2002). Partial or complete dissociation curves for various synthetic (Vycor and sol–gel) mesoporous silicas have been reported previously by other workers (Uchida *et al.* 1999, 2002; Seshadri *et al.* 2001; Wilder *et al.* 2001*a*, *b*; Seo *et al.* 2002; Smith *et al.* 2002*a*, *b*, 2004; Wilder & Smith 2002; Zhang *et al.* 2002, 2003; Seo & Lee 2003; Dicharry *et al.* 2005), and show very similar characteristics.

For the purposes of interpretation, we can re-plot heating curve data in terms of the volume of pore hydrate formed relative to growth/dissociation temperature depression. Figure 4 shows a plot of

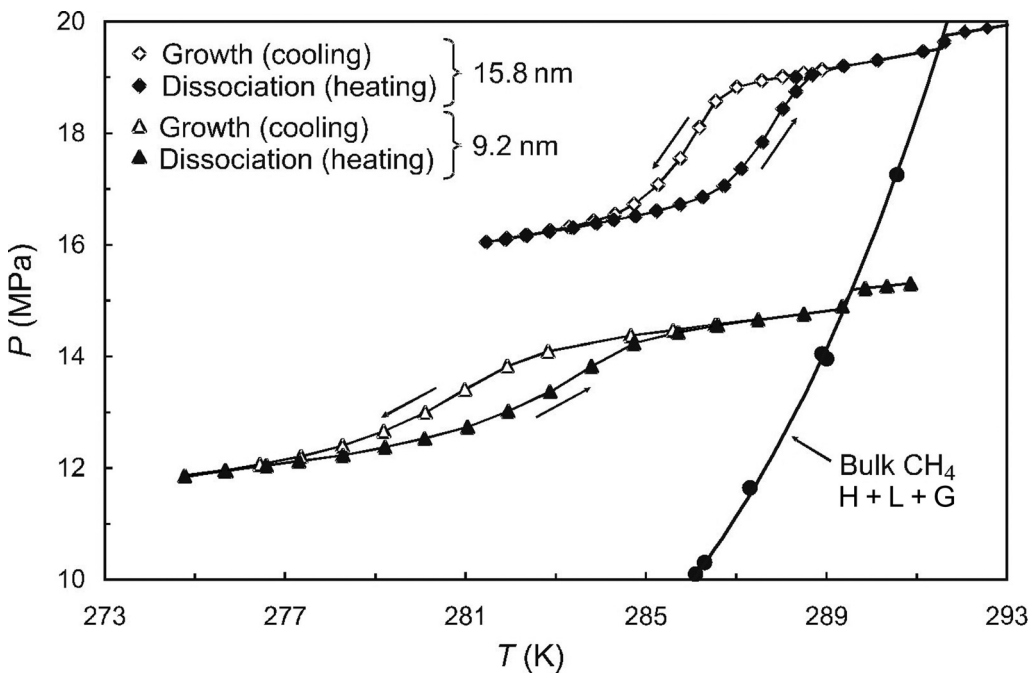


**Fig. 3.** Examples of primary methane hydrate growth and dissociation loop *PT* data for the 9.2 nm and 15.8 mean pore diameter CPG silicas. Bulk $CH_4$ data: polynomial fit to Deaton & Frost (1946), McLeod & Campbell (1961).

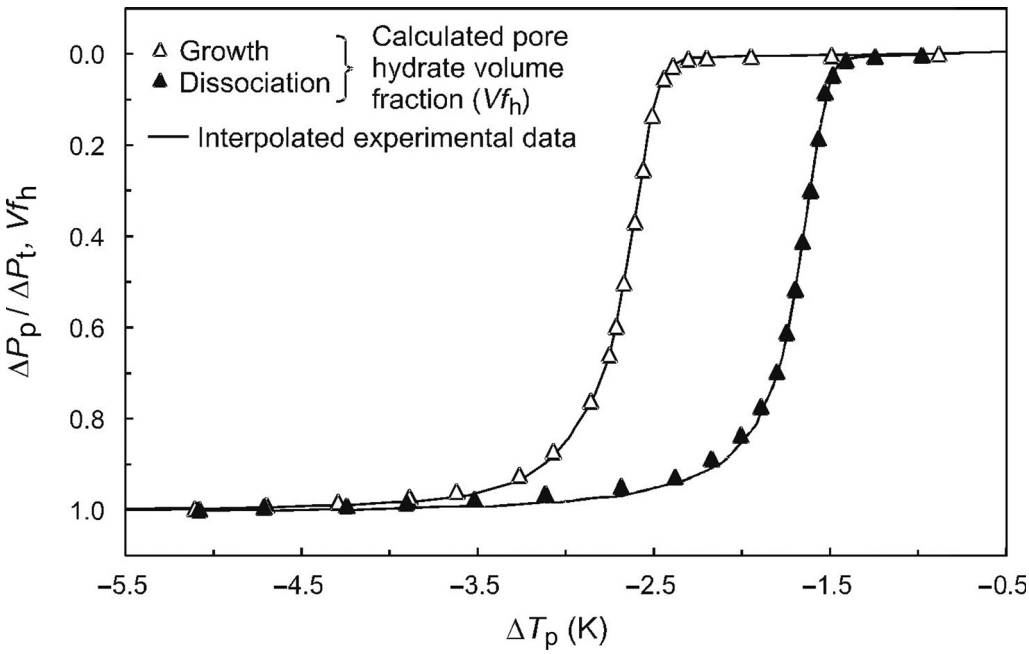


**Fig. 4.** Plot of $\Delta T_p$ v. $\Delta P_p/\Delta P_t$ (experimental data) and calculated volume fraction of pore hydrate ($Vf_h$) present for selected experimental points (30.6 nm sample). The fraction of total pressure change associated with pore hydrates essentially equals the volume fraction of pore hydrate formed at any point.

$\Delta T_p$ v. $\Delta P_p/\Delta P_t$ for the 30.6 nm sample where, as illustrated in Figure 2, $\Delta T_p$ is the temperature depression of hydrate growth/dissociation conditions from the bulk methane hydrate phase boundary, $\Delta P_p$ is the change in pressure associated with pore hydrate formation at any point and $\Delta P_t$ is the total change in pressure associated with pore hydrate formation. Also plotted for comparison is the calculated volume fraction of pore gas hydrate ($Vf_h$) present at each point. Hydrate volume fractions were calculated by standard iterative mass balance/volume methods assuming a methane hydration ratio of 1 : 6 (Handa 1986; Lievois *et al.* 1990; Ciscone *et al.* 2005). As can be seen, the faction (of total) pressure change associated with pore hydrates for each point is essentially equal to the volume fraction of pore hydrate present at that condition. Thus, in further analyses, we can consider that as a good approximation, $\Delta P_p/\Delta P_t = Vf_h$.

As our interest lies in the relationship between pore radius and hydrate growth/dissociation conditions, we could theoretically use equation (1) to convert $\Delta T_p$ to equivalent $r$, allowing the examination of data in terms of $Vf_h$ v. $r$. However, this would require the assumption of specific pore/solid–solid interface shapes for both solid formation and melting conditions, as defined by the shape factor, $F$, in equation (1). To avoid this assumption, we can compare growth and dissociation in terms of acting capillary pressure, $P_c$, at $\Delta T_p$. $P_c$ can be calculated by substituting the right hand side of the Young–Laplace equation:

$$P_c = P_s - P_l = \frac{F\gamma_{sl}\cos\theta}{r} \tag{2}$$

where $P_s$ is the pressure of the solid (hydrate) phase and $P_l$ the pressure of the liquid phase, into equation (1) and rearranging to yield:

$$P_c = \frac{\Delta T_p}{T_b} \cdot \rho_l \Delta H_{sl} \tag{3}$$

Figure 5 presents pore hydrate volume fractions as a function of calculated capillary pressure during growth and dissociation for all the three CPG silicas. As can be seen, hysteresis loops for all samples show very similar characteristics, with primary growth (increasing $P_c$) and dissociation (decreasing $P_c$) *PT* pathways being of sigmoidal form, consistent with Gaussian-like pore size distributions. As would be expected, capillary pressures increase as a function of pore diameter, the 9.2 nm mean pore diameter sample having the highest capillary pressure range/greatest degree of hydrate inhibition.

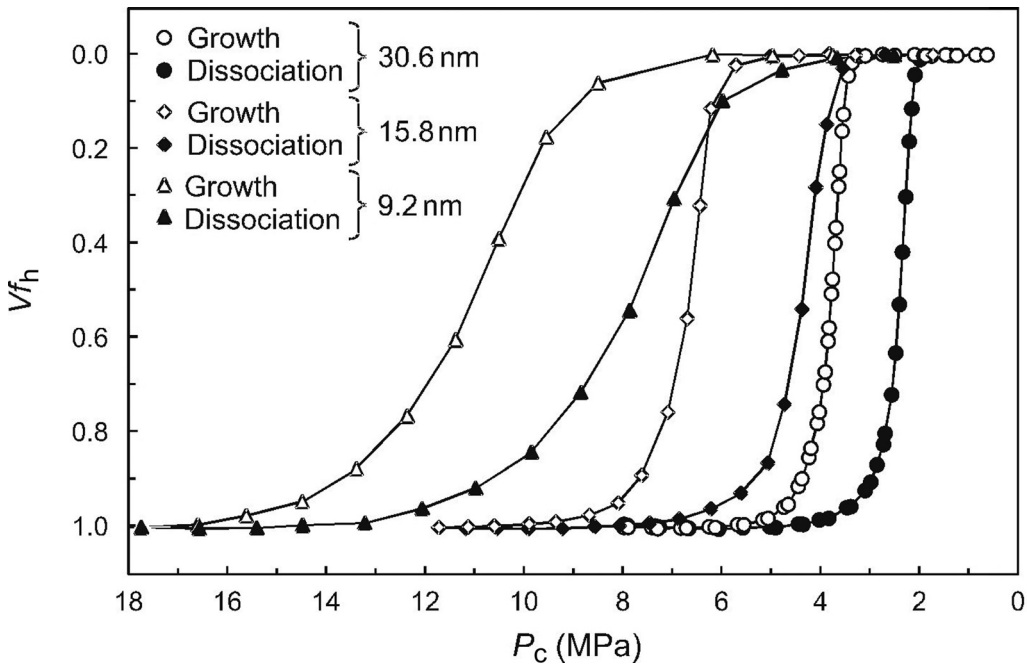


**Fig. 5.** Volume fraction pore hydrate versus capillary pressure for primary growth and dissociation loop data for all CPG silica samples studied.

By initiating cooling from any point on the primary dissociation curve, or conversely, by heating from any point on the primary growth curve, a variety of secondary characteristic 'scanning' growth/dissociation *PT* pathways may be followed, as illustrated in Figures 6 and 7 for the 30.6 nm sample. We adopt the term 'scanning' because it is generally used to describe similar curves in gas adsorption/desorption studies of mesoporous materials (Mason 1982, 1988). As for primary growth/dissociation pathways, scanning curves are irreversible, leading to an infinite number of possible, but consistent and repeatable *PT* pathways within the primary loop, depending on initial conditions. This behaviour, although often not investigated (primary loops only being reported), has been studied in detail for gas adsorption/desorption (Mason 1988). However, as far as we are aware, there is little (if any) comparable data for solid–liquid equilibria available.

## Origins of hysteresis

We have shown previously (Anderson *et al.* 2003*b*) that, in agreement with the Gibbs–Thomson equation (1), mean pore diameter $CH_4$, $CO_2$ and $CH_4$–$CO_2$ clathrate hydrate dissociation (and ice melting data) for CPG samples shows a linear correlation between $\Delta T_p/T_b$ and $1/r$, giving a consistent and thermodynamically predictable relationship between hydrate dissociation conditions and pore size (Llamedo *et al.* 2004). However, data presented here show that hydrate growth conditions are depressed to significantly lower temperatures compared with dissociation, resulting in a distinct *PT* hysteresis between opposing transitions. To predict this behaviour, and assess its potential implications for hydrates in the seafloor environment, then it is first necessary to establish its origins.

The causes of hysteresis in porous media are still poorly understood (Everett 1954; Mason 1982, 1988; Christensen 2001; Ravikovitch & Neimark 2002). A significant part of the problem lies in the complexity of pore structures, which may comprise various heterogeneous (at the pore scale) pore geometries, a wide range of pore diameters and varying degrees of interconnectivity. To precisely predict hysteresis behaviour for a particular medium, we can imagine that it might be necessary to have an intimate knowledge of the pore space in terms of all these factors. A detailed analysis of CPG pore structures is beyond the scope of this paper; however we can speculate as to the origins of the observed hysteresis patterns based on accepted capillary theory.

The most basic pore model assumes single, simple pore shapes, such as spheres or cylinders. To introduce pore interconnectivity as a factor, it

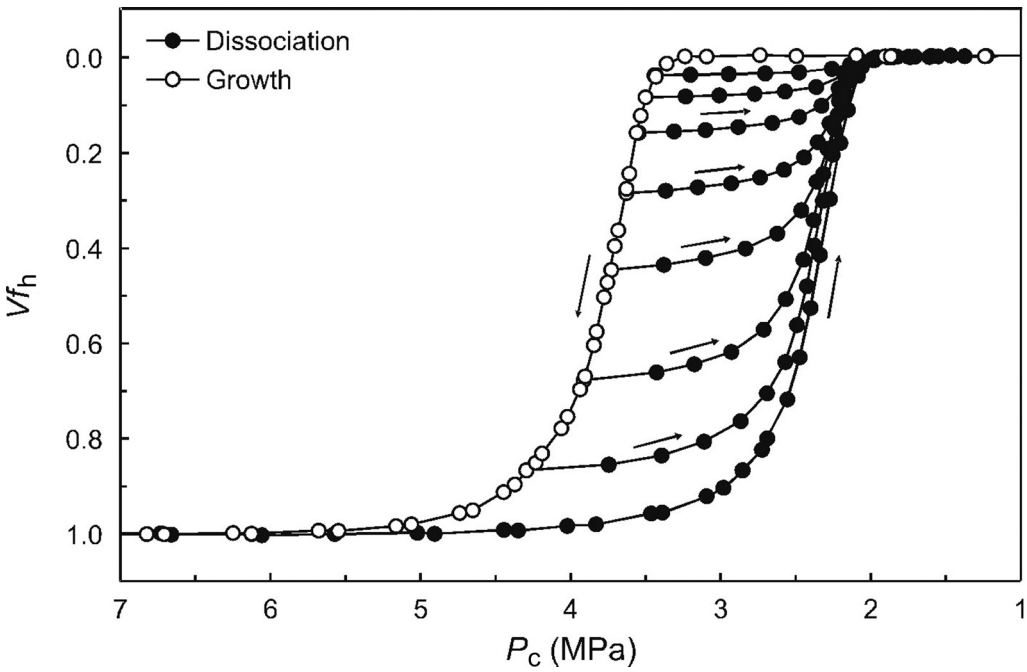


**Fig. 6.** Volume fraction pore hydrate versus calculated capillary pressure for secondary scanning dissociation curves originating from the primary growth curve (30.6 nm mean pore diameter CPG sample).

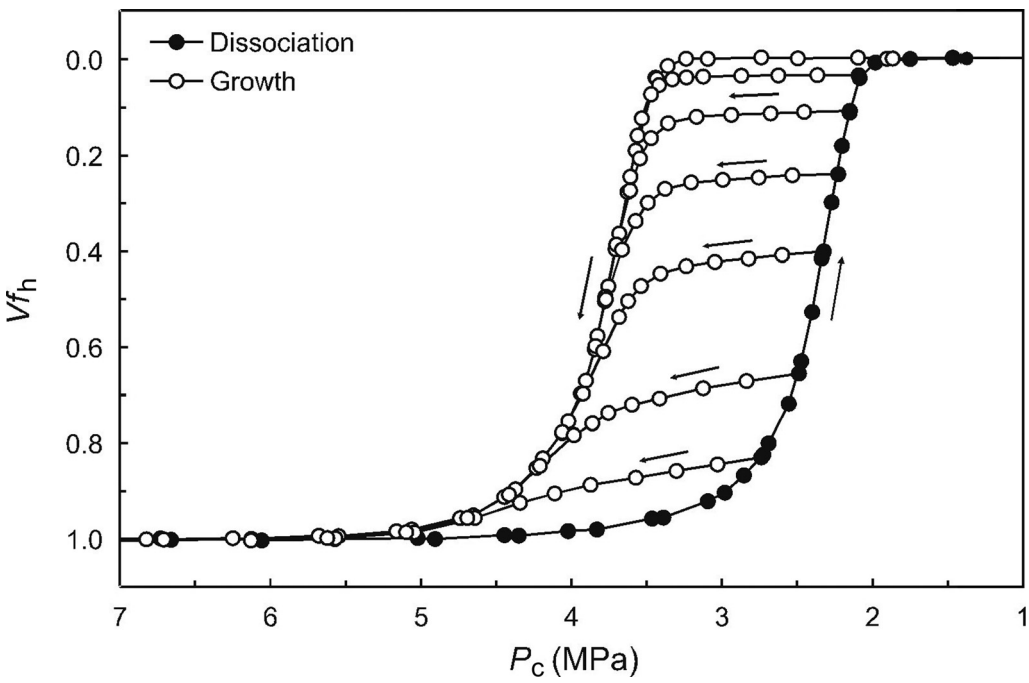


**Fig. 7.** Volume fraction hydrate versus capillary pressure for secondary scanning growth curves originating from the primary dissociation curve (30.6 nm mean pore diameter CPG sample).

is common to consider a matrix of spherical-like nodes connected by cylindrical-like bonds (Mason 1988; Vidales *et al.* 1995). Based on scanning electron microscopy (SEM) images and molecular dynamics simulations (Gelb & Gubbins 1998), this type of model might give a reasonable representation of controlled pore glasses. In such a media, we can consider two particular factors which may contribute to hysteresis: (1) pore geometry, and (2) pore blocking.

### *Influence of pore geometry*

The geometry of a pore will have a major influence on the interface curvatures of confined phases, thus capillary pressures. For a media containing a notable component of cylindrical-like capillaries, hysteresis could potentially arise due to differences in solid–liquid interface curvatures during crystallisation and melting (Brun *et al.* 1977; Jallut *et al.* 1992; Faivre *et al.* 1999). The interface shape factor $F$ in equations (1) and (2) is defined by the solid–liquid interfacial curvature, $\kappa$, in terms of the pore radius by:

$$F = \kappa r \tag{4}$$

with $\kappa$ being defined by:

$$\kappa = \left(\frac{1}{r_1} + \frac{1}{r_2}\right) \tag{5}$$

where $r_1$ and $r_2$ are the two orthogonal radii that describe the interface at any point. For solid–liquid transitions in a spherical pore, $r_1$ and $r_2$ are equal during both solid growth and melting, thus mean curvature is $2/r$ for both cases. In contrast, as shown in Figure 6, for solid growth in cylindrical pores, if the solid–liquid interface is considered a hemispherical cap, then $r_1$ and $r_2$ are equal, giving a mean curvature of $2/r$. However, for melting, although $r_1$ remains constant, $r_2$ is infinite ($1/r_2 \rightarrow 0$), thus total curvature is $1/r$. A curvature of $1/r$ implies that the solid–liquid interface should not retreat through a pore upon melting, but rather the solid cylinder should instantaneously melt along its length when stability conditions for the appropriate pore radius are surpassed. This concept is analogous to gas/oil phase 'snap-off' in (water-wet) cylindrical pores of reservoir rocks as hydrocarbon saturation is reduced (Blunt 1997; Hui & Blunt 2000). We can account for this geometrical control in equations (1) and (2) by modifying appropriately; $F = 2$ for growth and 1 for dissociation.

Based on the above, we can envisage that a media containing a notable proportion of cylindrical-like capillaries should display a temperature (or pressure) hysteresis between solid-phase crystallization and decomposition. Applying this to the results for CPG detailed here, then, if cylindrical pores are the cause of the observed hysteresis, we might expect to observe that for an appropriate volume of fraction of pore hydrate, $Vf_h$, capillary pressure during hydrate growth, $P_{c,g}$, should be around double that for dissociation, $P_{c,d}$. From examination of the data presented in Figures 5–7, this is clearly not the case: capillary pressures during hydrate growth are considerably less than double that for dissociation, with $P_{c,g}$ to $P_{c,d}$ ratios decreasing with decreasing sample mean pore diameter.

Figure 8 shows a plot of $P_{c,g}$ v. $P_{c,d}$ for equal pore volume fractions of clathrate present. As can be seen, rather than $P_{c,g}$ being a multiple of $P_{c,d}$ (e.g. $P_{c,g} = 2P_{c,d}$) the relationship appears to be additive, that is, $P_{c,g} = P_{c,d} + x$, where $x$ is relatively constant for a specific CPG sample, but variable between samples, and decreases with mean pore diameter. Furthermore, if CPG is composed primarily of cylindrical-like capillaries, then we might expect that, upon heating from the primary growth curve, dissociation would begin only when the primary dissociation curve was reached, that is, hydrate which had grown into progressively smaller cylindrical pores to radius $r$ at $P_{c,g}(r)$ would only melt on heating when $P_{c,d}(r)$ was reached, with $P_{c,g} = XP_{c,d}$ ($X$ being 2 for an ideal cylinder as detailed). However, Figure 6 shows that hydrate dissociation begins in earnest almost immediately on heating from the primary growth curve, suggesting the presence of a significant proportion of pores with interface curvatures which are approximately equal on growth and dissociation, that is, spherical-like rather than cylindrical.

Data thus suggest that differences in interface curvature for growth and dissociation in cylindrical capillaries is not the sole mechanism responsible for the observed hysteresis. However, results do not preclude this as being at least partly responsible for the phenomena. For any given point on the primary growth curve, the capillary pressure is at least double that for the associated point of complete pore hydrate dissociation achieved on heating, as can be seen in Figures 6 and 9. As shown in Figure 9, data suggest that $P_{c,g}$ is close to $2P_{c,d}$ at the points of initial hydrate growth (on the primary growth curve) and final hydrate dissociation, respectively (although determining these conditions exactly is problematic as the amount of hydrate present in the pores becomes infinitesimally small and within the error in measured pressure change).

As noted, the fact that dissociation begins almost immediately on heating from the primary growth curve suggests hydrate in pores with mean interface curvatures (thus capillary pressures) which are similar on growth and dissociation,

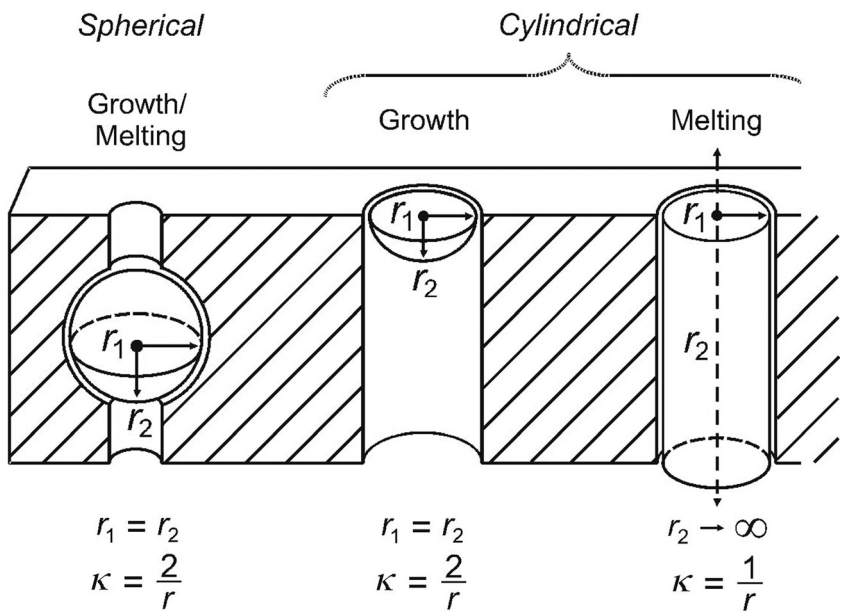


**Fig. 8.** Illustration of the difference in interface curvatures for hydrate growth and dissociation in ideal spherical and cylindrical pores.

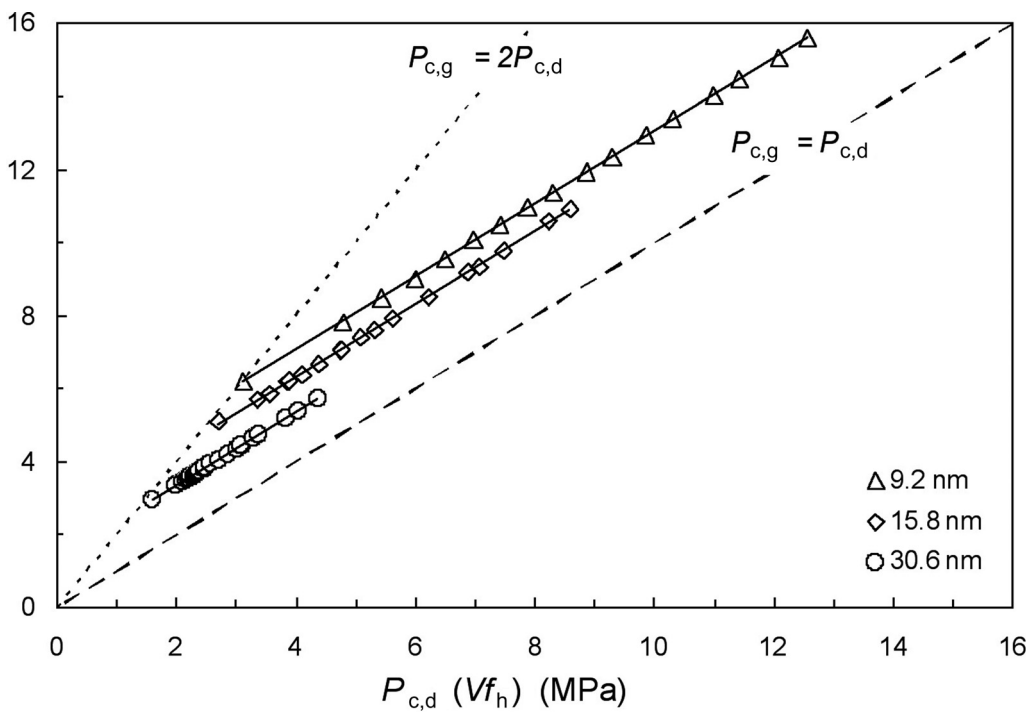


**Fig. 9.** Plot of capillary pressure during hydrate ($P_{c,g}$) growth v. that for dissociation ($P_{c,d}$) for equal volume fractions ($Vf_h$) of pore hydrate present. At the points corresponding to initial growth/final dissociation ($P_{c,g}$ and $P_{c,d}$ minima), $P_{c,g}$ approaches $2P_{c,d}$.

that is, spherical-like pores. Hydrate in these pores should theoretically grow and melt at the same capillary pressure condition (or $\Delta T_p$). However, data in Figure 6 shows that this is not the case as $P_c$ at conditions for growth is much higher than that for dissociation for the same volume of hydrate present. In light of this, it is necessary to consider mechanisms which could cause the observed hysteresis that are not primarily related to the interface curvature/geometry of individual pores. A potential candidate for this is 'pore blocking'.

### *Pore blocking effects*

Pore blocking has been proposed by a number of authors as a primary cause of the hysteresis commonly observed for liquid–vapour phase transitions in porous media (Mason 1988; Ravikovitch & Neimark 2002). The classic example of pore blocking is that for 'ink-bottle' pores (large pores with narrow necks) which cannot drain (desorb) until the capillary pressure reaches that needed for vapour phase entry into the narrow pore neck. We can apply this same theory to solid–liquid transitions if we consider the solid hydrate phase penetrating liquid-filled pores as analogous to vapour phase penetration during desorption. Figure 10 shows a simple illustration of the mechanisms by which pore blocking could be envisaged to occur in a hydrate–liquid system.

If we consider a large pore of radius $r_a$ accessible to the bulk only via smaller pores of $r < r_a$, then, in the absence of heterogeneous nucleation within the pore space, hydrate growth conditions for the large pore will be determined by the capillary entry pressure required for clathrate penetration of the smallest access pore throat, in this case of radius $r_d$. This means that hydrate growth in the large pore will take place at a temperature much lower than its 'unblocked' equilibrium freezing/melting temperature, as predicted by equation (1). On heating, however, equilibrium dissociation conditions of hydrate in the large pore will depend on its own radius, $r_a$. If we consider this blocking mechanism acting in a porous medium with a wide distribution of interconnected pores of different radii, it can be envisaged that many pores of large radius may only be accessible to growth fronts propagating from the bulk by means of narrower pore throats. In this case, it would be expected that a significant hysteresis would develop between solid growth and melting temperatures.

In Figure 11, data for selected individual secondary dissociation (scanning) curves for the 30.6 nm

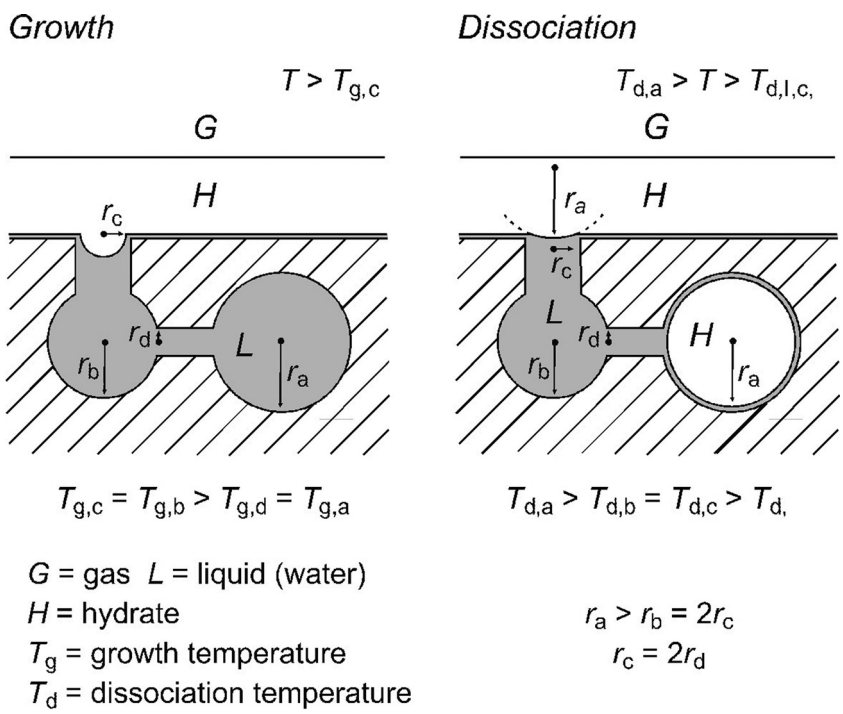


**Fig. 10.** Illustration of pore blocking effects in interconnected pores of different radii and geometry (cylindrical or spherical). See text for discussion.

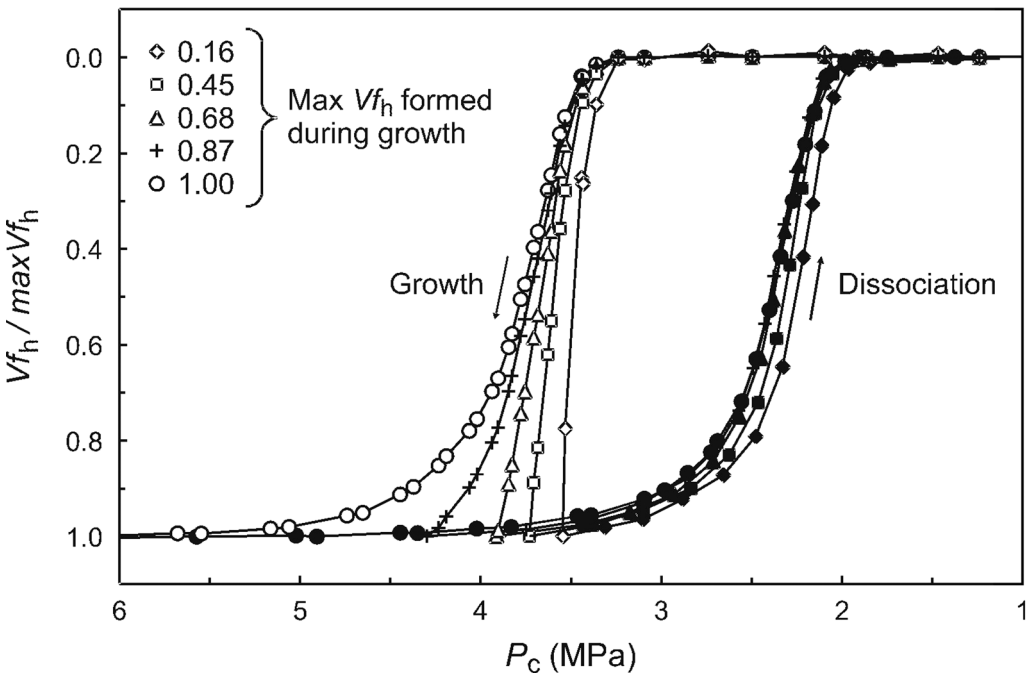


**Fig. 11.** Normalized volume fractions of pore hydrate versus capillary pressure for selected secondary scanning dissociation curves originating on the primary growth curve. Plotted $Vf_h$ data are normalized individually based on maximum pore volume fraction of hydrate (max $Vf_h$) formed during growth (open symbols) on the primary growth curve before dissociation was initiated along a scanning curve (solid symbols).

sample have been normalized with respect to appropriate maximum volume fraction of hydrate formed on the primary growth curve in each case. Also shown are associated primary growth curve data for each. Heating curves essentially represent dissociation across the cumulative pore size/volume distributions (PSD) for pores in which hydrates have formed during cooling along the primary growth curve to the starting $P_c$ condition. We can see from Figure 11 that, irrespective of initial starting conditions on the primary growth curve, dissociation curves are strikingly similar, suggesting that, in each case, hydrate decomposition takes place across a PSD closely representative of the media as a whole. As the $P_c$ (thus $\Delta T_p$) reached during primary growth is increased, so a larger volume of hydrate formed in pores of smaller radii (increased capillary pressure) is added to the total hydrate volume, as evidenced by associated secondary scanning dissociation curves shifting to higher capillary pressures. This pattern strongly supports pore blocking as a cause of the observed hysteresis.

Based on the above, we can envisage that the primary growth curve represents hydrate penetration into the media as a function of the pore throat entry radius distribution and associated accessible, 'freezable' volume (i.e. pore volume of water which can be converted to gas hydrate). As the system is cooled, the capillary entry pressure for progressively smaller 'access' pore throats is achieved, allowing the growth front to penetrate further from the bulk into the media, converting an additional fraction of the pore volume to hydrate at each stage, with each volume fraction converted being closely representative of the pore size distribution as a whole.

Secondary growth scanning curves originating on the primary dissociation curve add support to a pore blocking model (Fig. 7). It can be envisaged that, during dissociation, hydrate in some large pores (dissociation temperatures not yet reached) should become isolated (e.g. consider the large pore of radius, $r_a$ in Fig. 10). On cooling, hydrate in these large pores will act as secondary sites for initiation of the hydrate growth front as it starts to penetrate back into the media. For many regions of the pore network, this may mean that the capillary pressure, thus $\Delta T_p$ required to initiate hydrate growth, is considerably less than that which would normally be required for conditions where the front penetrates from the bulk alone (i.e. primary growth curve conditions). As such, re-growth on secondary scanning curves should be more pronounced and occur at lower $P_{c,g}$ than for the

primary growth curve. This behaviour is observed in Figure 7; for secondary scanning growth curves initiated on the primary dissociation curve, hydrate formation (increasing $Vf_h$) at lower $P_c$ becomes increasingly pronounced as starting $P_c$ is reduced (i.e. less hydrate dissociated before regrowth initiated), with the 'knees' which represent breakthrough pressures becoming increasingly flattened.

## Significance for seafloor hydrate systems

It is beyond the scope of this paper to investigate in detail the potential effects of the observed hysteresis on gas hydrate growth dissociation conditions in the natural sedimentary environment. However, some preliminary comments can be made based on the results presented here.

Fine-grained silts, muds and clays which commonly host gas hydrates can have quite narrow mean pore diameters (0.1 μm) (Griffiths & Joshi 1989; Clennell *et al.* 1999). For curvatures of $2/r$ (spherical) and $1/r$ (cylindrical), our results suggest that pore diameters of 0.1 μm could reduce hydrate stability (dissociation) by 15 m (*c.* 0.5 °C) and 30 m (*c.* 0.9 °C) respectively in areas of moderate geothermal gradient (30 °C/km). This is a significant potential displacement. Depending on the extent to which pore blocking (and the locus of hydrate formation within pore space) plays a role, then temperature restrictions for hydrate growth could be notably greater.

Results strongly suggest that hydrate formation in narrow pores is characterized by progressive solid growth front penetration from the bulk or larger voids into the media. Front progression (as temperature is decreased or pressure increased) will be dependent upon the distribution of narrow pore throats relative to associated accessible voids. One would imagine these factors to be quite media-specific. This, and the fact that pore hydrate dissociation conditions are independent of interconnectivity, suggests the pore space of natural sediments must be characterized in terms of both pore throat entry radius distribution and specific pore radius/volume distribution if we are to accurately predict both hydrate growth and dissociation conditions for a particular media.

Regarding the proposed pore blocking phenomena, it should be noted that the process requires nucleation to be restricted within pores. For the mesoporous materials examined here (maximum pore diameters of 0.05 μm or 50 nm), it seems that growth front propagation is favoured over nucleation, although it might be expected that, in much larger pores/voids, heterogeneous nucleation may be the preferred mechanism for hydrate crystallization.

## Conclusions

We have reported the results of a detailed experimental investigation of methane hydrate growth and dissociation conditions in synthetic mesoporous silica glasses. Data demonstrates that hydrate formation and decomposition in narrow pore networks are characterized by a distinct hysteresis between opposing transitions–hydrate growth taking place at temperatures considerably lower (or pressures higher) than those of dissociation. The hysteresis is an equilibrium phenomenon, and takes the form of irreversible, repeatable closed primary bounding growth/dissociation *PT* loops within which various characteristic secondary growth and dissociation specific 'scanning' *PT* pathways may be followed, depending on initial conditions. Similar hysteretic phenomena have been reported for ice growth and melting in the pores of cement pastes, and the behaviour appears to be closely analogous to that commonly observed for liquid–vapour transitions (gas adsorption–desorption) in mesoporous materials.

A detailed experimental analysis suggests that hysteresis arises primarily as a result of pore blocking during hydrate growth, although differences in interface curvatures during solid growth and decomposition resulting from pore geometry constraints (e.g. cylindrical pores) are likely to also contribute.

Results show that hydrate growth is characterized by capillary pressure-controlled progressive solid growth penetration from the bulk (or larger pores/voids) into the pore network as a function of decreasing temperature (increasing capillary pressure) with heterogeneous nucleation in pores not being favoured. In contrast, pore hydrate dissociation conditions appear to be principally controlled by interface curvatures as determined by individual pore geometry. As this behaviour has been observed for both synthetic and (more) natural (i.e. cement pastes composed of a variety of natural minerals), for both hydrates and ice, it is very likely that similar phenomena will occur during hydrate growth and dissociation in fine-grained natural sediments.

This work was funded by the UK Engineering and Physical Sciences Research Council (EPSRC grant no. EP/D052556), whose support is gratefully acknowledged. The authors would like to thank Jim Pantling and Colin Flockhart for manufacture and maintenance of experimental equipment.

## References

Aladko, E. Y., Dyadin, Y. A. *et al.* 2004. Dissociation conditions of methane hydrate in mesoporous silica gels in wide ranges of pressure and water content. *Journal of Physical Chemistry B*, **108**, 16540–16547.

ANDERSON, R., LLAMEDO, M., TOHIDI, B. & BURGASS, R. W. 2003*a*. Experimental measurement of methane and carbon dioxide clathrate hydrate equilibria in mesoporous silica. *Journal of Physical Chemistry B*, **107**, 3507–3514.

ANDERSON, R., LLAMEDO, M., TOHIDI, B. & BURGASS, R. W. 2003*b*. Characteristics of clathrate hydrate equilibria in mesopores and interpretation of experimental data. *Journal of Physical Chemistry B*, **107**, 3506–3509.

BOOTH, J. S., ROWE, M. M. & FISHER, K. M. 1996. Offshore gas hydrate sample database with an overview and preliminary analysis. *US Geological Survey Open File Report*, **96–272**.

BLUNT, M. J. 1997. Pore level modeling of the effects of wettability. *SPE Journal*, **2**, 494–510.

BREWER, P. G., FRIEDERICH, C. & PELTZER, E. T. 1999. Direct experiments on the ocean disposal of fossil fuel $CO_2$. *Science*, **284**, 943–945.

BRUN, M., LALLEMAND, A., QUINSON, J.-F. & EYRAUD, C. 1977. A new method for the simultaneous determination of the size and shape of pores: The thermoporometry. *Thermochimica Acta*, **21**, 59–88.

CHRISTENSEN, H. K. 2001. Confinement effects on freezing and melting. *Journal of Physics: Condensed Matter*, **13**, R95–133.

CISCONE, S., KIRBY, S. H. & STERN, L. A. 2005. Direct measurements of methane hydrate composition along the hydrate equilibrium boundary. *Journal of Physical Chemistry B*, **109**, 9468–9475.

CLENNELL, M. B., HOVLAND, M., BOOTH, J. S., HENRY, P. & WINTERS, W. J. 1999. Formation of natural gas hydrates in marine sediments. Part 1: Conceptual model of gas hydrate growth conditioned by host sediment properties. *Journal of Geophysical Research B*, **104**, 22985–23003.

DEATON, W. M. & FROST, E. M. 1946. Gas hydrates and their relation to the operation of natural gas pipelines. *US Bureau of Mines Monograph*, **8**, 101.

DICHARRY, C., GAYET, P., MARION, G., GRACIAA, A. & NESTEROV, A. N. 2005. Modeling heating curve for gas hydrate dissociation in porous media. *Journal of Physical Chemistry B*, **109**, 17205–17211.

DICKENS, G. R. 2003. Methane hydrates in quaternary climate change – the clathrate gun hypothesis. *Science*, **299**, 1017.

DORE, J. C., WEBBER, J. B. W. & STRANGE, J. H. 2004. Characterisation of porous solids using small-angle scattering and NMR cryoporometry. *Colloids and Surfaces A*, **241**, 191–200.

ENÜSTÜN, B. V., ŞENTÜRK, H. S. & YURDAKUL, O. 1978. Capillary freezing and melting. *Journal of Colloid and Interface Science*, **65**, 509–516.

EVERETT, D. H. 1954. A general approach to hysteresis. Part 3: A formal treatment of the independent domain model of hysteresis. *Transactions of the Faraday Society*, **50**, 1077–1096.

FAIVRE, C., BELLET, D. & DOLINO, G. 1999. Phase transitions of fluids confined to porous silicon: A differential calorimetry investigation. *European Physical Journal B*, **7**, 19–36.

GELB, L. D. & GUBBINS, K. E. 1998. Characterization of porous glasses: Simulation models, adsorption isotherms, and the BET analysis method. *Langmuir*, **14**, 2097–2111.

GRIFFITHS, F. J. & JOSHI, R. C. 1989. Change in pore-size distribution due to consolidation of clays. *Geotechnique*, **39**, 159–167.

HANDA, Y. P. 1986. Compositions, enthalpies of dissociation, and heat capacities in the range 85 to 270 K for clathrate hydrates of methane, ethane, and propane, and enthalpy of dissociation of isobutane hydrate, as determined by a heat-flow calorimeter. *Journal of Chemical Thermodynamics*, **18**, 915–921.

HANDA, Y. P. & STUPIN, D. 1992. Thermodynamic properties and dissociation characteristics of methane and propane hydrates in 70-Å-radius silica gel pores. *Journal of Physical Chemistry*, **96**, 8599–8603.

HENRY, P., THOMAS, M. & CLENNELL, M. B. 1999. Formation of natural gas hydrates in marine sediments. Part 2: Thermodynamic calculations of stability conditions in porous sediments. *Journal of Geophysical Research B*, **104**, 23005–23022.

HUI, M.-H. & BLUNT, M. J. 2000. Pore-scale modeling of three-phase flow and the effects of wettability. *SPE*, **59309**.

HUNTER, K. A. 1999. Direct disposal of liquefied fossil fuel carbon dioxide in the ocean. *Marine and Freshwater Research*, **50**, 755–760.

JACKSON, C. L. & MCKENNA, G. B. 1990. The melting behavior of organic materials confined in porous solids. *Journal of Chemical Physics*, **93**, 9002–9011.

JACKSON, C. L. & MCKENNA, G. B. 1996. Vitrification and crystallization of organic liquids confined to nanoscale pores. *Chemistry of Materials*, **8**, 2128–2137.

JALLUT, C., LENOIR, J., BARDOT, C. & EYRAUD, C. 1992. Thermoporometry: Modeling and simulation of a mesoporous solid. *Journal of Membrane Science*, **68**, 271–282.

KVENVOLDEN, K. A. 1999. Potential effects of gas hydrate on human welfare. *Proceedings of the National Academy of Sciences of the USA*, **96**, 3420–3426.

LEE, S.-Y. & HOLDER, G. D. 2001. Methane hydrates potential as a future energy source. *Fuel Processing Technology*, **71**, 181–186.

LIEVOIS, J. S., PERKINS, R., MARTIN, R. J. & KOBAYASHI, R. 1990. Development of an automated, high pressure heat flux calorimeter and its application to measure the heat of dissociation and hydrate numbers of methane hydrate. *Fluid Phase Equilibria*, **59**, 73–97.

LLAMEDO, M., ANDERSON, R. & TOHIDI, B. 2004. Thermodynamic prediction of clathrate hydrate dissociation conditions in mesoporous media. *American Mineralogist*, **89**, 1264–1270.

MASON, G. 1982. The effect of pore space connectivity on the hysteresis of capillary condensation in adsorption-desorption isotherms. *Journal of Colloid and Interface Science*, **88**, 36–46.

MASON, G. 1988. Determination of the pore-size distributions and pore-space interconnectivity of Vycor porous glass from adsorption–desorption hysteresis capillary condensation isotherms. *Proceedings of the Royal Society of London A*, **415**, 453–486.

MAX, M. D. (ed.). 2000. *Natural Gas Hydrate in Oceanic and Permafrost Regions*. Kluwer Academic: Dordrecht.

MCLEOD, H. O. & CAMPBELL, J. M. 1961. Natural gas hydrates at pressures to 10,000 psia. *Journal of Petroleum Technology*, **222**, 590–594.

MILKOV, A. V., SASSEN, R., NOVIKOVA, I. & MIKHAILOV, E. 2000. Gas hydrates at minimum stability depths in the Gulf of Mexico: Significance to geohazard assessment. *Gulf Coast Association of Geological Societies Transactions*, **50**, 217–224.

MORISHIGE, K. & KAWANO, K. 1999. Freezing and melting of water in a single cylindrical pore: The pore-size dependence of freezing and melting behavior. *Journal of Chemical Physics*, **110**, 4867–4872.

ØSTERGAARD, K. K., ANDERSON, R., LLAMEDO, M. & TOHIDI, B. 2002. Hydrate phase equilibria in porous media: Effect of pore size and salinity. *Terra Nova*, **14**, 307–312.

PAULL, C. K., MATSUMOTO, R., WALLACE, P. J. & DILLON, W. P. (eds). 2000. *Proceedings of the Ocean Drilling Program: Scientific Results*, **164**. Ocean Drilling Program, College Station, TX.

RAVIKOVITCH, P. & NEIMARK, A. V. 2002. Experimental determination of different mechanisms of evaporation from ink-bottle type pores: Equilibrium, pore blocking, and cavitation. *Langmuir*, **18**, 9830–9837.

RENNIE, G. K. & CLIFFORD, J. J. 1977. Melting of ice in porous solids. *Journal of the Chemical Society, Faraday Transactions 1*, **73**, 680–689.

RUPPEL, C. 1997. Anomalously cold temperatures observed at the base of the gas hydrate stability zone on the U.S. passive Atlantic margin. *Geology*, **25**, 699–702.

SCHULSON, E. M., SWAINSON, I. P., HOLDEN, T. M. & KORHONEN, C. J. 2000. Hexagonal ice in a hardened cement. *Cement and Concrete Research*, **30**, 191–196.

SEO, Y. & LEE, H. 2003. Hydrate phase equilibria of the ternary $CH_4 + NaCl +$ water, $CO_2 + NaCl +$ water and $CH_4 + CO_2 +$ water mixtures in silica gel pores. *Journal of Physical Chemistry B*, **107**, 889–894.

SEO, Y., LEE, H. & UCHIDA, T. 2002. Methane and carbon dioxide hydrate phase behaviour in small porous silica gels: Three phase equilibrium determination and thermodynamic modelling. *Langmuir*, **18**, 9164–9170.

SESHADRI, K., WILDER, J. W. & SMITH, D. H. 2001. Measurements of equilibrium pressures and temperatures for propane hydrate in silica gels with different pore size distributions. *Journal of Physical Chemistry B*, **105**, 2627–2631.

SMITH, D. H., WILDER, J. W. & SESHADRI, K. 2002*a*. Methane hydrate equilibria in silica gels with broad pore size distributions. *AIChE Journal*, **48**, 393–400.

SMITH, D. H., WILDER, J. W. & SESHADRI, K. 2002*b*. Thermodynamics of carbon dioxide hydrate formation in media with broad pore size distributions. *Environmental Science and Technology*, **36**, 5192–5198.

SMITH, D. H., SESHADRI, K., UCHIDA, T. & WILDER, J. W. 2004. Thermodynamics of methane, propane and carbon dioxide hydrates in porous glass. *AIChE Journal*, **50**, 1589–1598.

SWAINSON, I. P. & SCHULSON, E. M. 2001. A neutron diffraction study of ice and water within a hardened cement paste during freeze–thaw. *Cement and Concrete Research*, **31**, 1821–1830

TOHIDI, B., BURGASS, R. W., DANESH, A., TODD, A. C. & ØSTERGAARD, K. K. 2000. Improving the accuracy of gas hydrate dissociation point measurements. *In*: HOLDER, G. D. & BISHNOI, P. R. (eds) *Gas Hydrate Challenges for the Future*. Annals of the New York Academy of Sciences, **912**, 924–931.

TRÉHU, A. M. & SHIPBOARD SCIENTIFIC PARTY. 2003. *Proceedings of the Ocean Drilling Program: Initial Reports*, **204**. Ocean Drilling Program, College Station, TX.

UCHIDA, T., EBINUMA, T. & ISHIZAKI, T. 1999. Dissociation conditions of methane hydrate in confined small pores. *Journal of Physical Chemistry B*, **103**, 3659–3662.

UCHIDA, T., EBINUMA, T., NAGAO, J. & NARITA, H. 2002. Effect of pore sizes on dissociation temperatures and pressures of methane, carbon dioxide and propane hydrates in porous media. *Journal of Physical Chemistry B*, **106**, 820–826.

UCHIDA, T., TAKEYA, S. *ET AL*. 2004. Decomposition of methane hydrates in sand, sandstone, clays, and glass beads. *Journal of Geophysical Research B*, **109**, B05206.

VIDALES, A. M., FACCIO, R. J. & ZGRABLICH, G. 1995. Capillary hysteresis in porous media. *Journal of Physics: Condensed Matter*, **7**, 3835–3843.

WILDER, J. W. & SMITH, D. H. 2002. Dependencies of clathrate hydrate dissociation fugacities on the inverse temperature and inverse pore radius. *Industrial and Engineering Chemistry Research*, **41**, 2819–2825.

WILDER, J. W., SESHADRI, K. & SMITH, D. H. 2001*a*. Modelling hydrate formation in media with broad pore size distributions. *Langmuir*, **17**, 6729–6735.

WILDER, J. W., SESHADRI, K. & SMITH, D. H. 2001*b*. Resolving apparent contradictions in equilibrium measurements for clathrate hydrates in porous media. *Journal of Physical Chemistry B*, **105**, 9970–9972.

ZHANG, W., WILDER, J. W. & SMITH, D. H. 2002. Interpretation of ethane hydrate equilibrium data for porous media involving hydrate–ice equilibria. *AIChE Journal*, **48**, 2324–2331.

ZHANG, W., WILDER, J. W. & SMITH, D. H. 2003. Methane hydrate–ice equilibria in porous media. *Journal of Physical Chemistry B*, **107**, 13084–13089.